Inorganic Chemistry

Article

pubs.acs.org/IC

$[Tl^{III}(dota)]^-$: An Extraordinarily Robust Macrocyclic Complex

Tamás Fodor,[†] István Bányai,[‡] Attila Bényei,[§] Carlos Platas-Iglesias,[∥] Mihály Purgel,[⊥] Gábor L. Horváth,[†,#] László Zékány,[†] Gyula Tircsó,[†] and Imre Tóth*[,†]

[†]Department of Inorganic and Analytical Chemistry, [‡]Department of Colloid and Environmental Chemistry, [§]Department of Physical Chemistry, University of Debrecen, H-4032 Debrecen, Egyetem tér 1, Hungary

[∥]Departamento de Química Fundamental, Facultade de Ciencias, Universidade da Coruña, Campus da Zapateira-Rúa da Fraga 10, 15008 A Coruña, Spain

[⊥]MTA-DE Homogeneous Catalysis and Reaction Mechanisms Research Group, H-4032 Debrecen, Egyetem tér 1, Hungary

[#]Institute of Innate Immunity, University Hospital, University of Bonn, 53127 Bonn, Germany

Supporting Information

ABSTRACT: The X-ray structure of $\{C(NH_2)_3\}[Tl(dota)]\cdot H_2O$ shows that the Tl^{3+} ion is deeply buried in the macrocyclic cavity of the $dota^{4-}$ ligand (1,4,7,10-tetraazacyclododecane-1,4,7,10-tetraacetate) with average Tl−N and Tl−O distances of 2.464 and 2.365 Å, respectively. The metal ion is directly coordinated to the eight donor atoms of the ligand, which results in a twisted square antiprismatic (TSAP′) coordination around Tl^{3+}. A multinuclear ^1H, ^{13}C, and ^{205}Tl NMR study combined with DFT calculations confirmed the TSAP′ structure of the complex in aqueous solution, which exists as the $\Lambda(\lambda\lambda\lambda\lambda)/\Delta(\delta\delta\delta\delta)$ enantiomeric pair. ^{205}Tl NMR spectroscopy allowed the protonation constant associated with the protonation of the complex according to $[Tl(dota)]^- + H^+ \leftrightarrows [Tl(Hdota)]$ to be determined, which turned out to be $pK^H_{Tl(dota)} = 1.4 \pm 0.1$. $[Tl(dota)]^-$ does not react with Br^-, even when using an excess of the anion, but it forms a weak mixed complex with cyanide, $[Tl(dota)]^- + CN^- \leftrightarrows [Tl(dota)(CN)]^{2-}$, with an equilibrium constant of $K_{mix} = 6.0 \pm 0.8$. The dissociation of the $[Tl(dota)]^-$ complex was determined by UV−vis spectrophotometry under acidic conditions using a large excess of Br^-, and it was found to follow proton-assisted kinetics and to take place very slowly (~10 days), even in 1 M $HClO_4$, with the estimated half-life of the process being in the 10^9 h range at neutral pH. The solution dynamics of $[Tl(dota)]^-$ were investigated using ^{13}C NMR spectroscopy and DFT calculations. The ^{13}C NMR spectra recorded at low temperature (272 K) point to C_4 symmetry of the complex in solution, which averages to C_{4v} as the temperature increases. This dynamic behavior was attributed to the $\Lambda(\lambda\lambda\lambda\lambda) \leftrightarrow \Delta(\delta\delta\delta\delta)$ enantiomerization process, which involves both the inversion of the macrocyclic unit and the rotation of the pendant arms. According to our calculations, the arm-rotation process limits the $\Lambda(\lambda\lambda\lambda\lambda) \leftrightarrow \Delta(\delta\delta\delta\delta)$ interconversion.

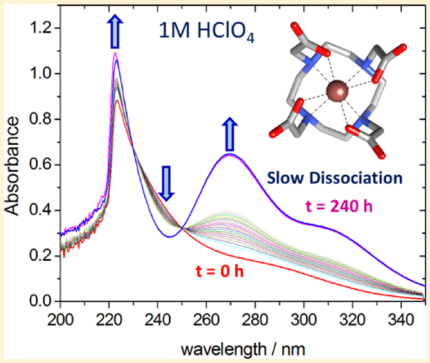

INTRODUCTION

The macrocyclic ligand 1,4,7,10-tetraazacyclododecane-1,4,7,10-tetraacetate ($dota^{4-}$) and its derivatives are known to be the most versatile ligands for medical imaging applications.[1] With a suitably sized cavity and four potentially coordinating pendant arms, this macrocyclic ligand forms complexes with many cations (i.e., Ln^{3+} ions,[2] Sc^{3+},[2] Y^{3+},[3] Ga^{3+},[4] Bi^{3+},[5] Ca^{2+},[6] Sr^{2+},[7] Zn^{2+},[8] and transition metal ions such as Fe^{3+},[9] Co^{2+},[4] Ni^{2+},[10] and Cu^{2+},[10]). The complexes are usually thermodynamically very stable[11] and kinetically quite inert.[12,13] These behaviors together make dota a very safe metal-binder because it can carry the metal component in biological fluids without risk of decomplexation, which would result in uncontrolled distribution of the components (i.e., metal ion and the ligand) in the biological system and may cause toxic effects or a decrease in the signal (e.g., relaxivity, luminescence, radioactivity). The advantages of providing high stability and inertness (often called kinetic stability in medical papers) are partly counterbalanced by the slow formation of metal−dota complexes.[14] While this is hardly a technical problem for stable isotopes, the long formulation time could be a crucial point for short-lived radioisotopes.[15]

Very intensive research during the last 2 to 3 decades has produced a trove of chemical knowledge about dota complexes, i.e., the stability constants,[12,14] formation and dissociation kinetics,[12−15] and structure in both the solid state[2,10] and solution[5,16] have been explored for many metal ions. A significant portion of the information that has allowed general conclusions to be established regarding dota complexes has been collected in lanthanide(III)−dota systems,[16] particularly the Gd^{3+} complex. This is related to the fact that $[Gd(dota)]^-$ is a very good and safe general (nonselective) magnetic resonance imaging (MRI) contrast agent (CA) widely used in clinical practice under the trade name Dotarem.

Received: February 26, 2015
Published: May 15, 2015

DOI: 10.1021/acs.inorgchem.5b00458
Inorg. Chem. 2015, 54, 5426−5437

The solution chemistry of the heaviest Group 13 element thallium is not very vital nowadays. Indeed, thallium was referred to as the forgotten element of the periodic table some time ago in a Ph.D. thesis.[17] Working with Tl^{3+} in aqueous solution is not a trivial task, as the trivalent ion has a strong tendency toward hydrolysis, so precipitation of Tl_2O_3 can occur even in acidic solutions (at pH 2.5). Tl^{3+} is also a strong oxidant, and organic ligands may reduce it to Tl^+.[18] The trivalent ion Tl^{3+} forms very stable complexes with amino-polycarboxylates such as edta (ethylendiaminetetraacetate), with the stability constant of log K = 37[19−22] being exceeded only by the constant of $[Co^{III}(edta)]^-$ (log K = 40.7).[23]

The coordination sites of Tl^{3+} are not completely saturated by the six donor atoms of the edta ligand and therefore quite stable $[Tl(edta)X]^{2-}$ ternary complexes with halide and pseudohalide anions have been detected (log $K_{mix[Tl(edta)X]^{2-}}$ = 2.30, 3.50, 2.70, and 8.72, where X = Cl^-, Br^-, SCN^-, and CN^-, respectively).[24] The $[Tl^{III}(edta)]^-$ complex is light-sensitive, as UV light induces oxidative decarboxylation of the ligand and formation of formaldehyde, CO_2, and Tl(I).[25] Recently, $[^{201}Tl^{III}(dota)]^-$ has been tested as a potential SPECT (single photon emission computed tomography) agent.[26] However, the structure of the $[Tl^{III}(dota)]^-$ complex and its thermodynamic stability has not been reported so far. Our present article summarizes new results on the equilibrium, kinetics, and structure of the Tl^{III}−dota system obtained with UV−vis and ^1H, ^{13}C, and ^{205}Tl NMR spectroscopy, single-crystal X-ray diffraction measurements, and DFT (density function theory) methods.

EXPERIMENTAL SECTION

Materials and Preparation of Solutions. The stock solution of $Tl(ClO_4)_3$ was prepared by anodic oxidation of $TlClO_4$. The electrolytic cell (see Supporting Information, Scheme S1) was filled with 6 M perchloric acid, and bubbles were removed mechanically from the cylinders and by opening the stopcock on the bridge to let any air out. A portion of solid $TlClO_4$ and a stirrer were added to the anode compartment. Electrolysis took place between a fine platinum mesh anode and a platinum plate cathode with an initial current strength of 120 mA. This gradually dropped to ∼80 mA during the process, which took a total of ∼51 h. The remaining portions of $TlClO_4$ were added as the anode compartment was slowly cleared of solids. In our case, 21 g of $TlClO_4$ was used, split into 7 g portions. Solutions of $[Tl(dota)]^-$ were prepared by (a) adding small portions of the $Tl(ClO_4)_3$ stock solution to a mildly basic (pH ∼ 8) solution of dota and dropwise addition of ∼20% NaOH to neutralize the acid (high acidity causes [TlH(dota)] to precipitate), (b) adding the required amount (1 equiv) of dota in one portion to a solution of $Tl(OOCCH_3)_3$ (prepared by mixing a portion of the $Tl(ClO_4)_3$ stock solution (1 equiv) and a 10-fold excess of acetic acid/sodium acetate buffer), and (c) following method (a) but using guanidine carbonate instead of NaOH. The pH of the resulting solutions was set to ∼4 to ensure that only $[Tl(dota)]^-$ was present (any excess of Tl(III) precipitates as Tl_2O_3). Photochemical decomposition was avoided by keeping the solutions in the dark.[27]

Analysis. Analysis of the $Tl(ClO_4)_3$ stock solution was performed as follows: A carefully measured volume of the stock solution (300 μL) was pipetted into a previously weighed titration flask and weighed. An excess of sodium chloride was added to avoid the hydrolysis of Tl(III), the sample was diluted with 5 mL of distilled water, and the acid content was determined by titration with 0.200 M NaOH, using methyl red as an indicator. Two milliliters of concentrated hydrochloric acid was added to re-acidify the solution, and the concentration of Tl^+ was determined by titration with 0.0100 M $KBrO_3$ at ∼95 °C. In the absence of Tl^+, methyl red is oxidized, turning the solution colorless, which signals the end point of the titration. The solution was brought to a low boil, and SO_2 was bubbled through for ∼30 min to reduce all thallium to Tl^+. (Excess SO_2 was removed by further boiling for ∼10 min.) The process for Tl^+ determination was repeated with 0.100 M $KBrO_3$.[28] This method yields the density, c_{Tl^+}, $c_{Tl(III)}$, and c_{H^+} data for the stock solution. The data for the stock solution used for the studies described herein were ρ = 1.72 g/cm^3, c_{Tl^+} = 9.25 mM, $c_{Tl(III)}$ = 1.192 M, and c_{H^+} = 3.96 M.

pH Measurements. pH values were measured by a Metrohm 6.0234.100 combined glass electrode connected to a Delta Ohm HD 8705 pH meter. The bridge electrolyte (3 M KCl) in the electrode was replaced with 1 M NaCl to avoid $KClO_4$ precipitation in the membrane. The pH meter was calibrated with KH-phthalate (pH 4.005) and KH_2PO_4−Na_2HPO_4 (pH 6.865) buffers, and the H^+ concentrations were calculated from the measured pH values by applying the method proposed by Irving et al.[29]

Spectrophotometry. UV−vis spectra were recorded in quartz cuvettes with a 1.0 mm path length using a Varian Cary 1E UV−visible spectrophotometer at 25 °C in the wavelength range 350−200 nm, with data points every 0.5 nm and a scan rate of 100 nm/min, unless otherwise stated. Short-term dissociation kinetics were followed by repeated recordings of spectra, with delay times of 1 h. The UV light was cut off from the sample during the delays to avoid photochemical decomposition. Long-term kinetics were followed by separate recordings, with delay times of 1 day or 1 week.

NMR Measurements. ^1H and ^{13}C spectra were recorded with a Bruker AM 400 spectrometer, at 400.1 and 100.6 MHz, respectively. In spite of lacking matching NMR probes capable of ^{205}Tl measurement, thallium spectra were obtained with a Bruker AM 360 spectrometer by inserting a 500 MHz BB probe and tuning the x-channel to the frequency of ^{205}Tl (207.8 MHz). This setup does not interact with ^1H or ^2H and does not enable locking or ^1H-decoupling to be used. Probe temperatures were kept at 25 (±0.1) °C if not stated otherwise. Calibration was performed using the signal of D_2O (4.79 ppm) for ^1H spectra, tetramethylsilane (0 ppm) for ^{13}C spectra, and 50 mM Tl(I)- and Tl(III)-perchlorate solutions (Tl^+: −4.72 ppm, Tl^{3+}: 2039 ppm) for ^{205}Tl spectra. Line-shape analysis was carried out with a homemade program written in MatLab, using the algorithm developed by Reeves and Shaw.[30] This program fits a signal-shape function simulating the change of coupling-free NMR signals caused by chemical exchange using modified Bloch equations (the coupling-free approximation implies that the same exchange rate is applied to both sets of signals). The relative positions of the two doublet signals used for the analysis were fixed, and the integrals (populations) and line widths within the doublets were assumed to be identical. Five parameters were estimated: two to define the baseline, one for the intensity, the frequency specific to the position of the signal, and the exchange rate constant. The calculated rate constants were then fitted to the Eyring−Polányi equation $[\ln(k/T) = -\Delta H^{\ddagger}/RT + \ln(k_B/h) + \Delta S^{\ddagger}/R$, where k is the rate constant, T is the absolute temperature, k_B is the Boltzmann constant, R is the ideal gas constant, h is the Planck constant, and $\Delta H^{\ddagger}$ and $\Delta S^{\ddagger}$ are the activation enthalpy and activation entropy, respectively].

Crystal Structure Analysis. The sodium salt of $[Tl(dota)]^-$ could not be crystallized in spite of repeated trials. Thus, we used the guanidine cation, which is known to aid the preparation of single crystals due to its strong ability to form hydrogen bonds.[31] Single crystals of $\{C(NH_2)_3\}[Tl(dota)]\cdot H_2O$ could be grown at the interface between 96% ethanol and a solution prepared by method (c) described above.

Diffraction intensity data collection was carried out at 293(2) K on a Bruker-Nonius MACH3 diffractometer equipped with a point detector using graphite-monochromated Mo Kα radiation (λ = 0.71073 Å). The structure was solved with the SIR-92 program[32] and refined by the full-matrix least-squares method on F^2. All non-hydrogen atoms were refined with anisotropic thermal parameters using the SHELXL-97 package.[33] Hydrogen atoms were located geometrically and refined in the rigid mode, except for hydrogen atoms of water molecules, which could be found in the difference electron density map. The remaining electron density peaks were found close to the Tl atom. Crystal data and structure refinement

DOI: 10.1021/acs.inorgchem.5b00458
Inorg. Chem. 2015, 54, 5426−5437

details are as follows: formula: $C_{17}H_{32}N_7O_9Tl$; MW: 682.87; crystal system: triclinic; space group: $P\bar{1}$; a = 7.498(10) Å; b = 12.406(5) Å; c = 12.800(4) Å; α = 91.01(1)°; β = 90.86(4)°; γ = 107.31(6)°; V = 1136.3(16) Å^3; Z = 2; D_{calc} = 1.996 g cm^{-3}; $F(000)$ = 672; μ = 7.17 mm^{-1}; reflections collected: 4909; unique reflections with $I > 2\sigma(I)$: 4117; parameters refined: 331; GOF on F^2 = 1.09; $R[F^2 > 2\sigma(F^2)]$ = 0.057; R_{int} = 0.046; w$R(F^2)$ = 0.156; $\Delta\rho_{max}$ and $\Delta\rho_{min}$ = 3.58 and −4.05 e Å^{-3}.

DFT Calculations. All calculations were performed in aqueous solution employing DFT within the hybrid GGA approximation with the B3LYP exchange-correlation functional[34] and the Gaussian 09 package.[35] Full geometry optimizations of the $[Tl(dota)]^-$ system were performed in aqueous solution without symmetry constraints. In these calculations, we used the relativistic effective core potential (RECP) of Ross et al. for Tl (CRENBL), which includes 68 electrons in the core, with the valence space (5d, 6s, and 6p) represented by an uncontracted (3s3p4d) basis set.[36] The ligand atoms were described using the standard 6-311+G(d,p) basis set. The stationary points found on the potential energy surfaces as a result of geometry optimizations were tested to represent energy minima rather than saddle points via frequency analysis.

The relative free energies of the different conformations of $[Tl(dota)]^-$ complexes were calculated in aqueous solution at the B3LYP/CRENBL/6-311+G(d,p) level, and they include non-potential-energy contributions (zero-point energies and thermal terms) obtained through frequency analysis. The arm-rotation and ring-inversion processes of $[Tl(dota)]^-$ were investigated by means of the synchronous transit-guided quasi-Newton method at the B3LYP/CRENBL/6-31+G(d,p) level.[37] The nature of the saddle points (one imaginary frequency) was characterized by frequency analysis. The free energy barriers calculated include non-potential-energy contributions obtained by frequency analysis.

The NMR shielding tensors of the $[Tl(dota)]^-$ system were calculated in aqueous solution using the B3LYP functional and the GIAO method.[38] In these calculations, the 6-311+G(d,p) basis set was used for the ligand atoms. For ^{13}C NMR chemical shift calculation purposes, the NMR shielding tensors of TMS were calculated at the same level.

Throughout this work, solvent effects were included by using the polarizable continuum model (PCM), in which the solute cavity is built as an envelope of spheres centered on atoms or atomic groups with appropriate radii. In particular, we used the integral equation formalism (IEFPCM) variant, as implemented in Gaussian 09.[39] The default values for the integration grid (75 radial shells and 302 angular points) and the SCF energy convergence criteria (10^{-8}) were used in all calculations.

RESULTS AND DISCUSSION

X-ray Crystal Structure. Crystals of $\{C(NH_2)_3\}[Tl(dota)]\cdot H_2O$ contain the $[Tl(dota)]^-$ complex, a guanidinium cation, and a water molecule. A view of the structure of the complex and bond distances of the metal coordination environment is provided in Figure 1. The Tl^{3+} ion is directly coordinated to the eight donor atoms of the ligand, with the metal coordination environment being best described as twisted square antiprismatic (TSAP).

The stereochemistry of eight- and nine-coordinate metal complexes of dota is well-documented; the coordination of the ligand to the metal ion introduces two sources of chirality, one associated with the conformation of the cyclen moiety [($\delta\delta\delta\delta$) or ($\lambda\lambda\lambda\lambda$)] and another related to the layout of the four acetate pendant arms [represented as Δ or Λ]. The combination of these two sources of helicity gives rise to four possible stereoisomers existing as two diastereoisomeric pairs of enantiomers. These enantiomeric pairs provide either a square antiprismatic [SAP, $\Delta(\lambda\lambda\lambda\lambda)/\Lambda(\delta\delta\delta\delta)$] or a TSAP [$\Lambda(\lambda\lambda\lambda\lambda)/\Delta(\delta\delta\delta\delta)$] coordination around the metal ion.[16e,40] Inspection

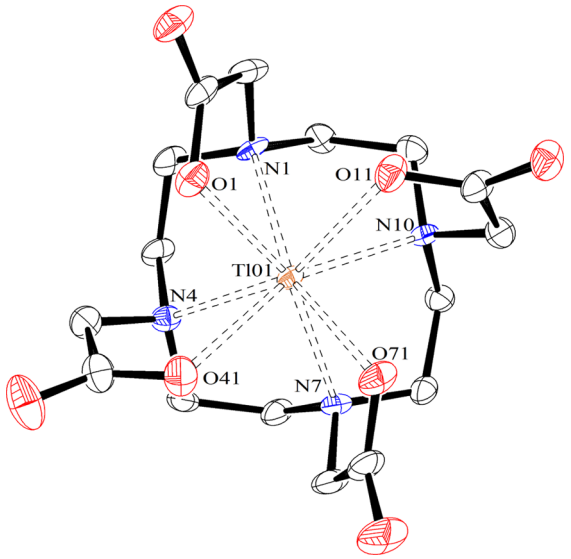

Figure 1. View of the structure of the $[Tl(dota)]^-$ complex present in crystals of $\{C(NH_2)_3\}[Tl(dota)]\cdot H_2O$. The ORTEP plot is at the 30% probability level. Bond distances (Å): Tl01−N1, 2.454(8); Tl01−N4, 2.497(9); Tl1−N7, 2.443(8); Tl01−N10, 2.458(9); Tl01−O1, 2.322(8); Tl01−O11, 2.438(8); Tl01−O41, 2.383(8); and Tl01−O71, 2.316(7).

of the structure of $\{C(NH_2)_3\}[Tl(dota)]\cdot H_2O$ shows that crystals contain the $\Lambda(\lambda\lambda\lambda\lambda)/\Delta(\delta\delta\delta\delta)$ enantiomeric pair, with the two enantiomers being centro-symmetrically related in accordance with the centro-symmetric character of space group $P\bar{1}$. Both the guanidinium cations and the water molecules are involved in hydrogen-bonding interactions with the oxygen atoms of the acetate groups of the ligand.

Dota-like complexes with the light Ln^{3+} ions are usually nine-coordinate, where the ligand acts as eight-dentate and one water molecule is in the inner coordination sphere. Eight coordination with the absence of a coordinated water molecule is typical for heavier Ln^{3+} ions such as Tm^{3+}. In both subgroups, SAP (Ln = Pr, Nd, Sm, Dy) and TSAP (Ln = Ce, Tm) geometries are found. Eight-coordinate complexes that lack the apical water molecule are often labeled as SAP′ and TSAP′ to differentiate them from the nine-coordinate SAP and TSAP complexes.[2a] $[Sc(dota)]^-$ adopts SAP′ geometry,[2a] in contrast with the TSAP′ coordination observed for $[Ca(dota)]^{2-}$, $[Bi(dota)]^-$, and $[Tm(dota)]^-$.[2a,5,6] In $[Tl(dota)]^-$, the coordination geometry around Tl^{3+} is TSAP′. The distinctive structural feature that discriminates SAP and SAP′ versus TSAP and TSAP′ structures is represented by the twist angle between the two square planes of the antiprism, the basal plane comprised of the four nitrogen atoms of the macrocycle, and the upper plane containing the four coordinated oxygen atoms of the pendant arms. The average twist angle observed for $[Tl(dota)]^-$ (25.4°) is close to that expected for a regular twisted square antitiprism (22.5°) and also similar to those found for other complexes having TSAP or TSAP′ structures (Table 1).

Table 1 provides a comparison of structural parameters reported in the literature for $[M(dota)]^-$ complexes (M = Sc^{3+},[2a] Tm^{3+},[2a] and Bi^{3+},[5]) with those of the Tl^{3+} analogue. Additionally, we have also included the corresponding data for selected $[M(dota)(H_2O)]^-$ complexes, with M = La[42] or Gd[9] as representative members of the earlier and middle members of the lanthanide series, respectively. The average M−O bond

DOI: 10.1021/acs.inorgchem.5b00458
Inorg. Chem. 2015, 54, 5426−5437

Table 1. Structural Parameters Observed for Selected $[M(dota)(H_2O)]^-$ and $[M(dota)]^-$ Complexes in the Solid State

M	La	Gd	Bi	Sc	Tm	Tl
ionic radius/Å[a]	1.216	1.107	1.17	0.87	0.994	0.98
M−O/Å[b]	2.467	2.368	2.538	2.150	2.279	2.365
M−N/Å	2.770	2.663	2.526	2.441	2.529	2.464
M−O/M−N	0.89	0.89	1.00	0.88	0.90	0.96
$M-Q_O$/Å[c]	0.728	0.715	1.112	1.007	1.064	1.252
$M-Q_N$/Å[d]	1.810	1.632	1.434	1.327	1.466	1.324
Q_O-Q_N	2.54	2.35	2.55	2.33	2.53	2.58
twist angle/deg[e]	23.2	38.5	25.9	41.1	24.4	25.4
isomer	TSAP	SAP	TSAP′	SAP′	TSAP′	TSAP′

[a]Ionic radii for coordination number eight (Bi, Sc, Tm, and Tl) or nine (La and Gd) taken from ref 41. [b]Average bond distances between the metal ion and the O atoms of the acetate arms. [c]Distance between the metal ion and the least-squares plane defined by the coordinated O atoms of acetate groups. [d]Distance between the metal ion and the least-squares plane defined by the N atoms of the macrocycle. [e]Calculated as the average value of the four torsion angles $N-C_N-C_O-O$, where N and O are the donor atoms defining a five-membered chelate ring and C_N and C_O represent the centroids of the Q_N and Q_O planes, respectively.

lengths are in the range of 2.54−2.15 Å, whereas the M−N distances range between 2.44 and 2.77 Å. The distances between the virtual planes defined by the four N atoms of the macrocycle (Q_N) and the four donor oxygen atoms of the pendant arms (Q_O) are ca. 2.53−2.58 Å for the complexes with TSAP and TSAP′ coordination and 2.33−2.35 Å for those with SAP and SAP′ geometries. Thus, the Q_O-Q_N distances for a given coordination polyhedron remain nearly unaffected by the nature of the metal ion or the presence of a coordinated water molecule,[43] whereas the position of the metal ion with respect to the Q_O and Q_N planes varies significantly. As expected, the $M-Q_O$ and $M-Q_N$ distances are substantially different for complexes having different coordination numbers (see, for instance, the values for La, Gd, and Tm in Table 1).[43] However, different $M-Q_O$ and $M-Q_N$ distances appear to be also related to important changes in the ratio of the M−O and M−N distances. The M−O/M−N ratio is very similar for complexes with hard metal ions La^{3+}, Gd^{3+}, Tm^{3+}, and Sc^{3+} (0.88−0.90), and it increases to 0.96 and 1.00 for the Tl^{3+} and Bi^{3+} complexes, respectively. For the latter complex, the M−O and M−N distances are nearly identical, whereas for the complexes with La^{3+}, Gd^{3+}, Tm^{3+}, and Sc^{3+}, the M−N bond distances are clearly longer than the M−O ones, and the $[Tl(dota)]^-$ complex presents an intermediate situation. A plot of the M−donor distances versus the ionic radii of the metal ions for the $[M(dota)]^-$ (M = Tm, Sc, Bi, or Tl) and $[Ca(dota)]^{2-}$ complexes (Figure 2) shows that both the M−N and M−O distances vary linearly with the ionic radius for the set of complexes with the hard metal ions Tm^{3+}, Sc^{3+}, and Ca^{2+}, whereas the Bi−O and Tl−O distances are longer, and the Bi−N and Tl−N distances are shorter, to the values expected from the linear trends. Thus, the soft nature of Tl^{3+} and Bi^{3+} according to the Pearson classification[44] provokes a strengthening of the coordination bonds with the softer N donor atoms, which results in a deeper penetration of the metal ion into the macrocyclic cavity. This effect becomes obvious when comparing the structural data reported in Table 1 for the complexes with Tm^{3+} and Tl^{3+}, which possess nearly identical ionic radii.

^{205}Tl NMR Spectroscopy. The ^{205}Tl nucleus has a nuclear spin of $I = {}^1/_2$ and very good sensitivity; therefore, ^{205}Tl NMR is quite useful to follow the formation of metal complexes in aqueous solution.[45] The ^{205}Tl NMR chemical shift range is huge and very sensitive to the oxidation state of the Tl ion in the particular compound.[46] The (proton coupled) ^{205}Tl NMR

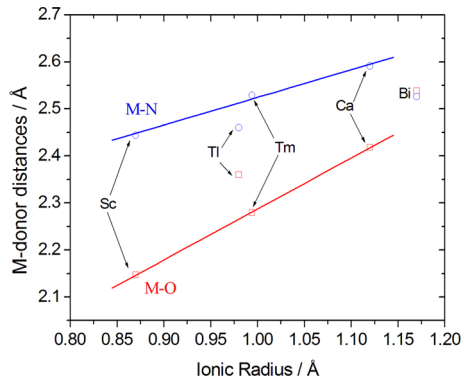

Figure 2. Variation of the M−N and M−O bond distances with the ionic radius in $[M(dota)]^-$ (M = Tm, Sc, Bi or Tl) and $[Ca(dota)]^{2-}$ complexes. The solid lines are linear fits of the data reported for the Ca^{2+}, Sc^{3+}, and Tm^{3+} complexes (see text).

spectrum of $[Tl(dota)]^-$ shows a single signal at δ = 2218 ppm with a chemical shift very similar to that measured earlier for $[Tl(edta)]^-$ (δ = 2301 ppm).[24] The positions of these signals are within the range expected for a Tl(III) compound, whereas the lack of a Tl(I) signal at around δ = 0 ppm indicates that there was no reduction of Tl(III) to Tl(I) during the preparation of $[Tl(dota)]^-$.[47] Furthermore, the absence of a signal due to Tl^{3+}_{aq} at δ = 2039 ppm confirms the full complexation of the metal ion by the ligand. The broad ^{205}Tl NMR signal observed at 298 K ($w_{1/2}$ = 2200 Hz) did not show multiplicity caused by ^{1}H spin−spin coupling to the protons of the dota ligand, which is likely related to the fluxional behavior of the complex (see below). However, the multiplicity due to ^{1}H−^{205}Tl coupling could be observed in the spectrum recorded at 289 MHz and 268 K, which is observed as a pseudononuplet with an apparent ^{1}H−^{205}Tl coupling constant of ∼500 Hz. This suggests that the ^{1}H−^{205}Tl coupling pattern in $[Tl(dota)]^-$ is dominated by the coupling to eight equatorial ring protons of the ligand.

^{205}Tl NMR shifts are very sensitive to small changes in the chemical environment around the Tl center and therefore can be used to follow the protonation/deprotonation of the $[Tl(dota)]^-$ complex by measuring the ^{205}Tl chemical shift at different pH values. Adding a strong acid to a solution of $[Tl(dota)]^-$ indeed causes significant changes in the observed ^{205}Tl NMR shift (Figure 3).

DOI: 10.1021/acs.inorgchem.5b00458
Inorg. Chem. 2015, 54, 5426−5437

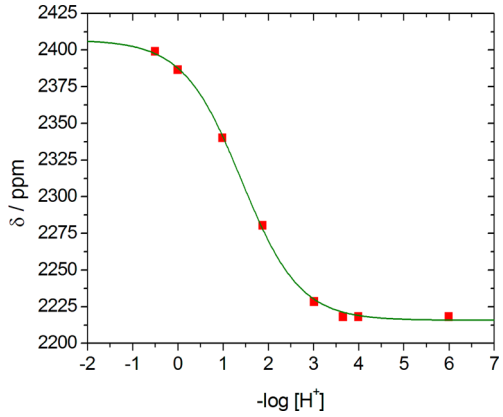

Figure 3. ^{205}Tl NMR shift of $[Tl(dota)]^-$ vs $-\log[H^+]$; measured data points (red) and fitted curve (green).

Plotting the chemical shift values vs pH shows a typical S-shaped curve with an inflection point at pH 1.4, which can be attributed to the protonation of $[Tl(dota)]^-$ according to

$$[Tl(dota)]^- + H^+ \rightleftharpoons [HTl(dota)] \quad (1)$$

$$K^H_{Tl(dota)} = [HTl(dota)]/[H^+][Tl(dota)^-] \quad (2)$$

The analysis of the $\delta - c_{H^+}$ curve provides $pK^H_{Tl(dota)} = 1.4 \pm 0.1$ ($\delta_{[HTl(dota)]} = 2405 \pm 3$ ppm and $\delta_{[Tl(dota)]} = 2216 \pm 1$ ppm). The protonation process most likely involves the protonation of one of the carboxylate arms. However, the accuracy of this constant was limited by several conditions: (1) it was not possible to keep the ionic medium constant, i.e., the most acidic sample contained 3 M perchloric acid; (2) the samples were not homogeneous. Formation of the charge-neutral [Tl(Hdota)] species at 1.0 and 0.1 M acid concentrations might be responsible for the precipitation of a white solid from the solution of $[Tl(dota)]^-$ under acidic conditions (see Experimental Section). Even so, the pK value could be calculated from the δ_{205Tl} vs pc_H curve without knowing the total concentration of the $[Tl(dota)]^-$ species. (3) At higher acid concentrations (3 M) the solution became homogeneous, which might be attributed to the formation of a charged diprotonated $[Tl(H_2dota)]^+$ species, with the two protonation steps being strongly overlapped. In any case, the evaluated protonation constant can be considered to be a reasonable estimate.

The ^{205}Tl NMR chemical shift of $[Tl(dota)]^-$ was constant in the pH range of 4−11, indicating the lack of formation of the $[Tl(dota)(OH)]^{2-}$ mixed complex. Considering the strong tendency of Tl(III) to undergo hydrolysis, this can be taken as a strong indication of a very tight coordination of the octadentate $dota^{4-}$ ligand to the central Tl^{3+} ion. For instance, in the case of $[Tl(edta)]^-$, the formation of a ternary hydroxo complex characterized by a pK = 6.0 has been reported.[20,24,48] The decreased reactivity of $[Tl(dota)]^-$ compared to that of $[Tl(edta)]^-$ is also evidenced by the very limited tendency of the former to form mixed complexes with bromide and cyanide ions. In comparison, $[Tl(edta)]^-$ forms relatively stable mixed complexes with the soft halide ions (i.e., $K_{Tl(edta)Br} = [Tl(edta)Br^{2-}]/[Tledta^-]\,[Br^-] = 10^{3.5}$),[24] whereas similar mixed complexes could not be detected for the $[Tl(dota)]^-$−Br^- system, even when using a large excess of halide over $[Tl(dota)]^-$ ($c_{Tl(dota)}$ = 5 mM, I = 1 M $NaClO_4$, pH ∼ 3, c_{Br} = 0−154 mM). Only the signal of $[Tl(dota)]^-$ at a constant shift (δ = 2218 ppm) was observed, whereas neither signals due to any mixed complex nor the signal of $[TlBr_4]^-$ at 1310 ppm that would indicate complex dissociation could be detected.[49]

The formation of a mixed $[Tl(dota)(CN)]^{2-}$ complex could be detected, however, using ^{205}Tl NMR experiments on the $[Tl(dota)]^-$−CN^- system. Addition of CN^- to a solution of $[Tl(dota)]^-$ resulted in the emergence of a new signal at δ = 2463 ppm ($w_{1/2}$ ∼ 2500 Hz) whose chemical shift was almost identical to that of the $[Tl(edta)(CN)]^{2-}$ complex (δ = 2460 ppm).[24] The intensity ratio of the signals assigned to $[Tl(dota)]^-$ and $[Tl(dota)(CN)]^{2-}$ allowed us to estimate a stability constant of ∼10 for the mixed complex. However, in order to obtain a more reliable equilibrium constant, pH-dependent ^{205}Tl NMR spectra were recorded. The pH dependence of the intensity ratio of the two signals indicated that the formation of the mixed complex was depressed by the protonation of cyanide to form HCN (Figure 4). The following simultaneous equilibria were considered:

$$[Tl(dota)]^- + CN^- \rightleftharpoons [Tl(dota)(CN)]^{2-} \quad (3)$$

$$K_{mix} = [Tl(dota)CN^{2-}]/[CN^-][Tl(dota)^-] \quad (4)$$

$$H^+ + CN^- \rightleftharpoons HCN \quad (5)$$

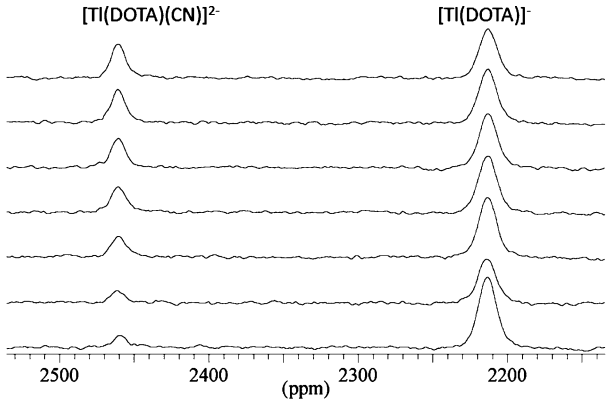

Figure 4. 207.1 MHz ^{205}Tl NMR spectra of samples with $c_{Tl(dota)}$ = 25 mM and c_{CN^-} = 100 mM at different pH values (from top to bottom): 10.62, 10.09, 9.76, 9.58, 9.40, 9.21, and 9.00.

Using the mass balance equations for the components of the equilibrium system and $K_{HCN} = 10^{9.09}$ (I = 1 M),[50] we obtained K_{mix} = 6.0 ± 0.8, a value that is 8 orders of magnitude lower than that of $[Tl(edta)(CN)^{2-}]$ ($K_{mix} = 10^{8.7}$). This difference is in line with a very tight wrapping of Tl^{3+} by the $dota^{4-}$ ligand. It is worth mentioning that our attempts to measure the ^{205}Tl−^{13}C coupling constant (expected to be similarly as large as the $^1J_{^{205}Tl-^{13}C}$ = 10.5 kHz for $[Tl(edta)(CN)]^{2-}$)[24] by ^{205}Tl NMR using ^{13}C-enriched NaCN failed, which is likely related to the fast cyanide exchange at the alkaline pH values required for the formation of the mixed complex.

Equilibrium and Kinetic Study by UV−Vis Spectroscopy. The stability constant of $[Tl(edta)]^-$ has been determined by a competition method using a large excess of both halide ligands and H^+.[20] In the case of $[Tl(dota)]^-$, an even greater stability is expected; furthermore, the macrocyclic complex forms very slowly in acidic solutions, which prevents the use of direct potentiometry for stability constant determination. Instead, we have used a competition method in which both a halide, namely bromide, and H^+ compete for

DOI: 10.1021/acs.inorgchem.5b00458
Inorg. Chem. 2015, 54, 5426−5437

Tl^{3+} and $dota^{4-}$, respectively, according to the following equilibrium characterized by the equilibrium constant, K_{comp}:

$$(n-1)H^+ + [HTl(dota)] + 4Br^- \rightleftarrows TlBr_4^- + H_ndota^{(4-n)-} \quad (6)$$

$$K_{comp} = \frac{[TlBr_4^-][H_ndota^{(4-n)-}]}{[HTl(dota)][H^+]^{n-1}[Br^-]^4} \quad (7)$$

Tl^{3+} behaves as a *soft* acid according to the classification of Pearson, as the stability of halide complexes increases from the light halide ions to the heavy ones. Therefore, iodide would be the strongest competing agent for Tl^{3+}. However, one has to consider redox reactions, i.e., Tl^{3+} can oxidize iodide to iodine while Tl^+ is formed (TlI_4^- is the only TlI_n^{+3-n} species detected in solution at high I^-/Tl^{3+} ratios).[45] Preliminary experiments have confirmed the immediate formation of iodine and therefore we have selected Br^- for the competition reactions.

Knowing the kinetic inertness of [M(dota)] complexes, suitable thermodynamic data can be extracted only from properly equilibrated competition systems. Thus, batch samples containing 0.5 mM $[Tl(dota)]^-$ and 0.5 M NaBr were prepared, varying the concentration of the acid in the range of 0.1, 0.3, 0.5, 0.8, and 1 M $HClO_4$ and keeping the total perchlorate concentration constant (at 1 M with $(Na^+ + H^+)ClO_4^-$). The dissociation of the complex, i.e., the formation of $[TlBr_4]^-$ was followed over time, recording spectra in the 200–350 nm range until the expected equilibration of the system (Figure 5).

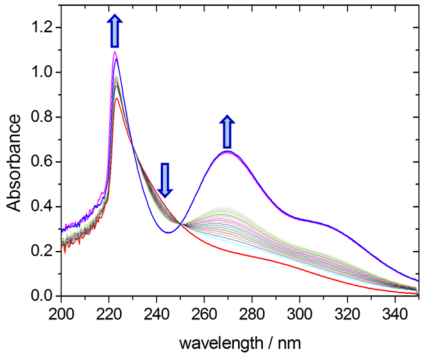

Figure 5. Time dependence of UV spectra attributed to the ligand-exchange reaction between [HTl(dota)] and Br^- in 1 M $HClO_4$: [HTl(dota)] (red, recorded at t_0) is slowly converted to $[Tl(Br)_4^-]$ (blue, recorded at 450 h; the absorbance value and the shape of the spectrum are in accordance with separate measurements of $[TlBr_4]^-$). Intermediate spectra were recorded at 1 h intervals for 19 h. Conversion is ~99% at 240 h (magenta).

The spectra shown in Figure 5 clearly show isosbestic point(s), which is in agreement with the presence of two species ([HTl(dota)] and $[Tl(Br)_4^-]$) in equilibrium with measurable absorbance during the 240 h experimental time in the system, in accordance with eq 6. However, the reaction is substantially slower in the less acidic samples, where the isosbestic points were not observed. This indicates that some kind of parallel side reaction is occurring under these conditions. This may be a slow redox reaction involving bromide ions and the Tl^{3+} ion in an out-of-cage intermediate in which the metal ion is coordinated only by carboxylate groups (as in the formation/dissociation intermediate observed for other dota complexes). We invested a high amount of time and energy trying to avoid this complication (exclusion of air from samples with argon, increasing temperature to shorten the equilibration time by conventional means and by using a microwave reactor) without any success in measuring the equilibrium constant defined by eq 7.

Finally, we decided to only use spectra recorded at low conversion to evaluate the kinetics of our Tl–macrocyclic complex by means of the initial rate method. Assuming that $[Tl(dota)]^-$ dissociates similarly to $[Gd(dota)]^-$,[12c] the following equations may be used to evaluate the kinetic data

$$-d[Tl(dota)]_t/dt = k_{obs}[HTl(dota)]_t \quad (8)$$

$$k_{obs} = k_0 + k_1[H^+] + k_2[H^+]^2 \quad (9)$$

where k_{obs} is the observed pseudo-first-order reaction rate constant, k_0 is the rate constant of spontaneous (or water-assisted) dissociation of the monoprotonated complex, and k_1 and k_2 are the constants of proton-assisted dissociation. The experimental results are shown in Figure 6. Curve fitting gives

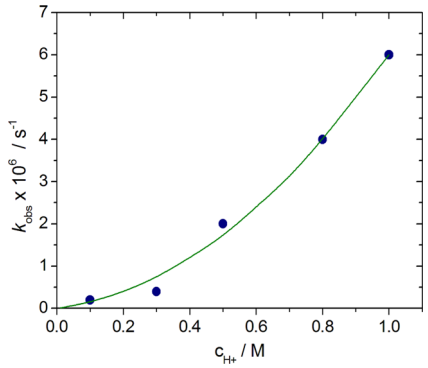

Figure 6. Plot of k_{obs} vs acid concentration in the Tl(III)–$dota^{4-}$–H^+–Br^- system: measured data points (blue) and fitted curve (green).

$k_0 = 0$ (fixed to 0 as the fitting of the dissociation kinetic data in a trial returned a small negative value with large error), $k_1 = (9 \pm 7) \times 10^{-7}$ s^{-1} M^{-1}, and $k_2 = (5 \pm 0.8) \times 10^{-6}$ s^{-1} M^{-2} values. The data shows quadratic dependence of k_{obs} on acidity with no detectable spontaneous dissociation, which is not surprising because spontaneous dissociation of the monoprotonated complex is expected to occur slower by several orders of magnitude than the acid-catalyzed dissociation (which is the dominant reaction pathway in the acid concentration range applied in the current study). The k_1 value also has a large uncertainty and may be a calculation artifact caused by the limited number of data points and their inaccuracy in the lower c_{H^+} range related to the above-mentioned side reactions during the very slow competition reaction. This kind of rate equation is in accordance with the related literature of dota complexes, i.e., the dissociation is a dominantly proton-assisted process (we have found some minor spectral changes that might be related to some interaction between [HTl(dota)] and the Br^- ion, but we could not quantitatively measure this probably small contribution to the dissociation kinetics). Using the $k_{obs} = k_1[H^+] + k_2[H^+]^2$ rate equation, one can calculate the half-life of the complex at different pH values. Half-life of $[Tl(dota)]^-$ is 32 h in 1 M $HClO_4$ and approximated to 5×10^9 h at pH 7.4. The latter value indicates that the dissociation of $[Tl(dota)]^-$ at physiological pH is negligible. To our surprise, however, the $[^{201}Tl(dota)]^-$ complex was recently found to decompose in

DOI: 10.1021/acs.inorgchem.5b00458
Inorg. Chem. 2015, 54, 5426–5437

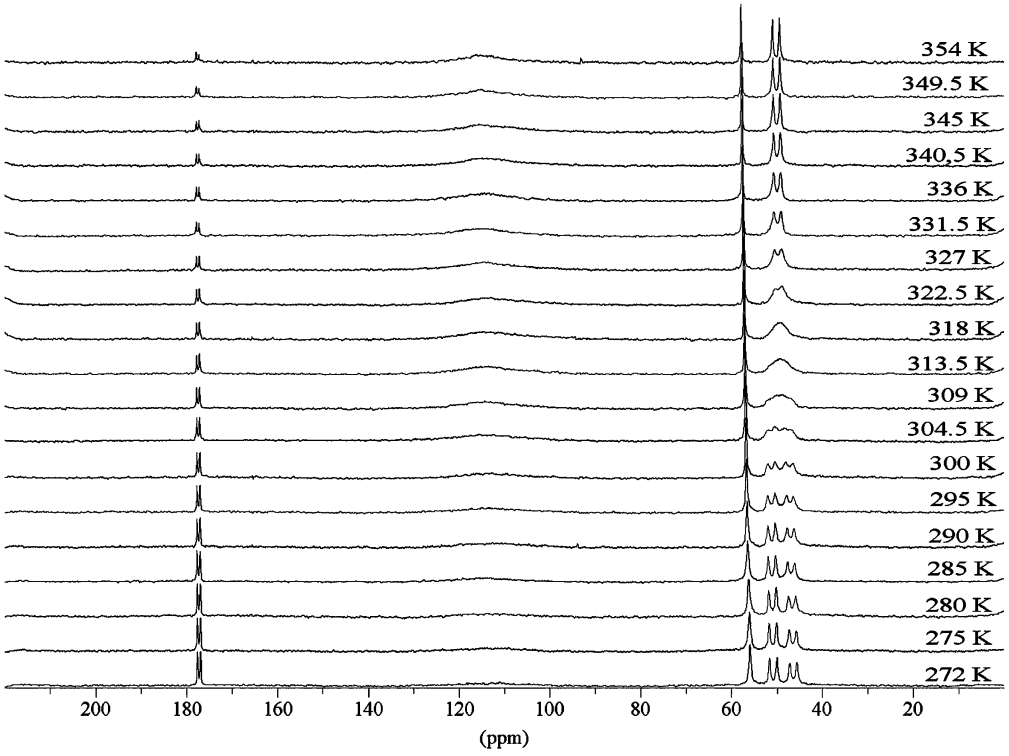

Figure 7. 100 MHz ^{13}C NMR spectra of a 0.1 M Na[Tl(dota)] solution in D_2O recorded at different temperatures in D_2O (pH 4).

vivo.[26] Our data suggests that this phenomenon is more likely to be caused by the bioreduction of Tl(III) in the samples rather than the dissociation of the $[Tl^{III}(dota)]^-$ complex. Tl^+ (showing similarity to K^+ both in size and complexation properties) likely forms a weak and labile complex with dota, making the dissociation of the reduced radioisotope from the complex easy.

^1H and ^{13}C NMR Spectroscopy. The ^1H NMR spectrum of $[Tl(dota)]^-$ presents six broad signals at room temperature: one doublet can be assigned to the protons of the acetate methylene groups and two doublets to those of the ring ($^3J_{^1H-^{205}Tl}$ scalar coupling splits these signals into doublets). The broadness of these signals is related to exchange processes occurring in solution. On the basis of the composition of the complex and that of the solution, the exchange is attributed to the intramolecular rearrangement of the complex. At higher temperatures, the signals sharpen and their structure becomes visible as a consequence of the acceleration of the exchange processes. This is also supported by ^{13}C NMR spectra, which at high temperatures show two signals in the aliphatic region: a singlet assignable to the acetate methylene carbons and a ^{205}Tl coupled doublet of the ring carbons (Figure 7). The carbon nuclei of the methylene groups of the pendant arms do not show ^{205}Tl coupling. This is likely caused by the combined effect of a two-bond coupling (through the nitrogen) and a three-bond coupling (through the carboxylate oxygen). These couplings may possess differing signs that presumably cancel each other.

The ^1H and ^{13}C NMR spectra recorded at low temperature (272 K) are relatively well-resolved and could be fully assigned with the aid of the homonuclear $^1H-^1H$ COSY and heteronuclear $^1H-^{13}C$ HSQC spectra (Figure 8; see Chart 1 for labeling). At this temperature, the ring carbon doublet splits into two, indicating the presence of two different chemical

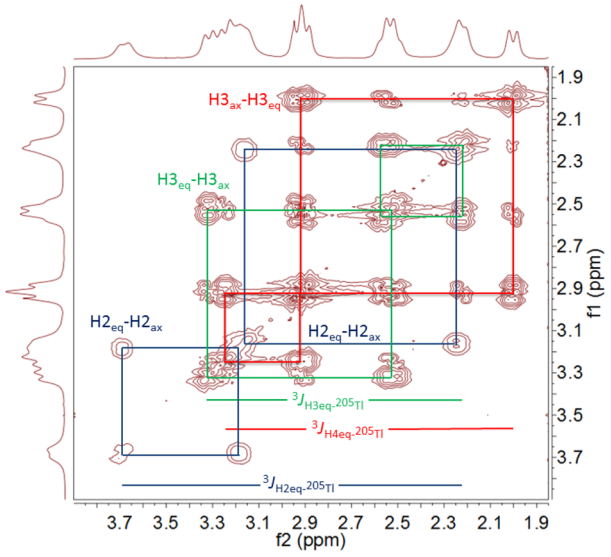

Figure 8. 400 MHz $^1H-^1H$ COSY spectrum of 0.1 M $[Tl(dota)]^-$ recorded in D_2O solution ($pD_{reading}$ = 4) at 272.5 K (see Chart 1 for labeling).

Chart 1. Ligand $dota^{4-}$ and the Numbering Scheme Used for NMR Spectral Assignment

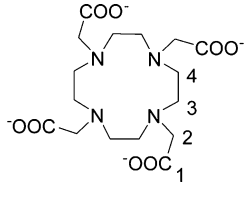

DOI: 10.1021/acs.inorgchem.5b00458
Inorg. Chem. 2015, 54, 5426−5437

Table 2. NMR Spectral Data of $[Tl(dota)]^-$

^1H	δ/ppm	$^3J_{H-^{205}Tl}$/Hz	^{13}C	δ/ppm	$^2J_{^{13}C-^{205}Tl}$/Hz	δ^{cald}_{TSAP} [b]	δ^{cald}_{SAP} [c]
$H2_{ax}$	3.19/3.16	11	C1	179.7	64	179.7	178.2
$H2_{eq}$	3.68[d]/2.24	574	C2	58.8	[a]	59.2	66.7
$H3_{ax}$	2.55/2.52	12	C3	53.6	161	51.8	56.9
$H3_{eq}$	3.32/2.23[e]	441	C4	49.2	156	48.4	55.2
$H4_{ax}$	2.91	<5					
$H4_{eq}$	3.24/2.00[f]	499					

[a]Not observed. [b]Chemical shifts of the TSAP′ isomer calculated at the B3LYP/CRENBL/6-311+G(d,p) level using the GIAO method. [c]Chemical shifts of the SAP′ isomer calculated at the B3LYP/CRENBL/6-311+G(d,p) level using the GIAO method. [d]$^2J_{2eq-2ax}$ = 13.5 Hz. [e]$^2J_{3eq-3ax}$ = 14.5 Hz. [f]$^2J_{4eq-4ax}$ = 14.0 Hz.

environments for the carbon nuclei of the macrocyclic moiety. The spectrum shows four signals: the ^{205}Tl-coupled doublet ($^2J_{^{205}Tl-^{13}C}$ = 64 Hz) of the carboxylate (−C═O) groups at δ = 179.7 ppm (C1), a singlet due to the $-CH_2-$ groups of the acetate pendant arms at 58.8 ppm (C2), and two ^{205}Tl-coupled doublets of the nonequivalent carbon atoms of the macrocycle ring centered at δ = 49.2 ($^2J_{^{205}Tl-^{13}C}$ = 156 Hz) and 53.6 ($^2J_{^{205}Tl-^{13}C}$ = 161 Hz) ppm. This pattern points to C_4 symmetry of the $[Tl(dota)]^-$ complex at low temperatures, whereas the spectra at temperatures higher than 320 K can be interpreted as an effective C_{4v} symmetry. The $^1H-^{13}C$ HSQC spectrum (Figure S2, Supporting Information) shows that each of the 3 carbon nuclei in the aliphatic region is coupled with 4 proton signals, with two of them showing very small chemical shift differences. This is clearly observed for the proton nuclei of the $-CH_2-$ groups of the acetate arms (H2). For these protons, one expects an AB spin system with a $^2J_{ax-eq}$ of ∼16 Hz. However, the coordination of the ligand to the Tl^{3+} ion creates an AB−X system, which splits each of the components of the AB spin systems into doublets due to the $^3J_{^1H-^{205}Tl}$ coupling. The $^1H-^1H$ COSY spectrum relates the signals at 3.19 and 3.68 ppm and those at 3.16 and 2.24 ppm, while no cross-peak is observed relating the signals at 3.68 and 2.24 ppm. All four of these signals are, however, correlated to the carbon atom of the acetate arms in the HSQC spectrum. Thus, the signals at 3.68 and 2.24 ppm are attributed to a single proton nucleus whose resonance is split by the coupling to ^{205}Tl. Analogous reasoning allowed us to assign the proton signals of the macrocyclic fragment (Table 2). Furthermore, the spin pattern of the signals allowed us to discriminate between axial (ax) and equatorial (eq) proton nuclei. Indeed, the different H−C−C−H dihedral angles relating axial and equatorial protons with the protons at a three-bond distance result in different coupling patterns, as expected by the Karplus relationship.[51,52] As a result, the equatorial protons provide small ^3J coupling constants, so their coupling patterns are dominated by the strong $^2J_{eq-ax}$ coupling (∼16 Hz). This is, for instance, the case of the signal at 2.00 ppm, which is observed as a pseudodoublet. On the contrary, axial protons give two strong couplings ($^2J_{ax-eq}$ and $^3J_{ax-ax}$) and a weak one ($^3J_{ax-eq}$), and they are observed as pseudotriplets (see, for instance, the signal at 2.91 ppm, Figure 8).

The $^3J_{^1H-^{205}Tl}$ coupling constants obtained from the analysis of the NMR spectra (Table 2) indicate that the equatorial protons provide coupling constants of ca. 440−575 Hz, whereas the coupling constants involving axial protons are rather small (<15 Hz). These coupling constants are very similar to the average coupling constant estimated from the splitting of the ^{205}Tl NMR spectrum recorded at low temperature (∼500 Hz, see above), which confirms the assignments given in Table 2. An inspection of the X-ray structure of $[Tl(dota)]^-$ shows that the equatorial protons provide average Tl−N−C−H_{eq} dihedral angles of 160.4−162.9°, whereas the corresponding values for axial protons Tl−N−C−H_{ax} take values of ca. 80−82°. These results indicate that the $^3J_{^1H-^{205}Tl}$ coupling constants follow the empirical relationship of Karplus ($^3J = A - B\cos\phi + C\cos 2\phi$, where ϕ is the dihedral angle and A, B, and C are empirical constants). A similar Karplus-like dependence was also observed for the spin density distributions in the paramagnetic $[Gd(dota)(H_2O)]^-$ complex and related systems.[53]

Solution Structure and Dynamics. The multinuclear NMR study described in the previous sections indicates an octadentate binding of the ligand to the Tl^{3+} ion in $[Tl(dota)]^-$. Furthermore, the X-ray structure suggests that this complex might adopt a TSAP′ structure in solution. In order to confirm this hypothesis, we performed theoretical calculations in aqueous solution at the B3LYP/CRENBL/6-311+G(d,p) level. Our calculations provide two energy minima that correspond to the expected SAP′ and TSAP′ isomers of the complex (Figure 9). A comparison of the experimental (X-ray) and calculated structure of the TSAP′ isomer indicates that our calculations provide molecular geometries in good agreement with the reference crystallographic data (Table 1). The main discrepancy between the experimental and calculated structures is the overestimation of the Tl−N distance by ca. 0.08 Å in the latter.

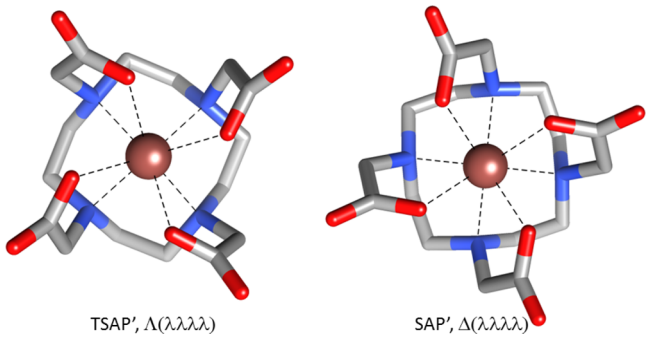

Figure 9. Geometries of the SAP′ and TSAP′ isomers of $[Tl(dota)]^-$ obtained from geometry optimizations in aqueous solution at the B3LYP/CRENBL/6-311+G(d,p) level. Hydrogen atoms are omitted for simplicity. Bond distances: Tl−N = 2.537 (TSAP′) and 2.528 Å (SAP′); Tl−O: 2.354 (TSAP′) and 2.341 Å (SAP′).

According to our calculations, the TSAP′ isomer is more stable than the SAP′ one by 15.2 kJ mol^{-1}, which is in line with the structure observed in the solid state. In order to confirm that $[Tl(dota)]^-$ adopts a TSAP′ structure in solution, we

DOI: 10.1021/acs.inorgchem.5b00458
Inorg. Chem. 2015, 54, 5426−5437

calculated the ^{13}C NMR chemical shifts of the SAP′ and TSAP′ isomers at the B3LYP/CRENBL/6-311+G(d,p) level. It has been shown that the magnetic shieldings calculated with the use of ECPs are not gauge invariant, which means that magnetic shieldings calculated with different origins are different. However, the errors introduced by this violation of the gauge invariance have been shown to amount to a few parts per million and therefore ^{13}C NMR shifts can be calculated by this method with reasonably good accuracy.[54,55] The ^{13}C NMR shifts calculated for the TSAP′ isomer are in very good agreement with the experimental data, with absolute deviations < 1.8 ppm, whereas much larger deviations between the experimental and calculated data are obtained for the SAP′ isomer (up to 6.8 ppm, see Table 2). Thus, our calculations confirm that the $[Tl(dota)]^-$ presents a TSAP′ structure in aqueous solution.

The increase of the symmetry observed in the ^{13}C NMR spectra upon increasing temperature can be explained by the higher rate of the chemical exchange between the two different chemical environments of the ring carbon atoms. Indeed, the doublet signals due to the carbon nuclei of the macrocyclic fragment are clearly separated at 272 K, indicating a slow exchange regime (Figure 7). The signals gradually broaden as the temperature increases, and they are hardly visible in the spectra recorded in the temperature range 300−320 K. The temperature of coalescence is ca. 315 K. The time-averaged signal (a Tl-coupled doublet) sharpens above 325 K, as expected for a two-site exchange system being in the fast exchange regime. It is worth noting, however, that the other two signals, i.e., the signals of the acetate arms, behave differently from the ring carbon signals. The half-widths for both signals are changing with temperature. However, the signal of aliphatic carbon atoms of the acetate arms becomes sharper with increasing temperature, which is typical of systems in fast exchange on the actual NMR time scale. One would expect splitting of the acetate peak into two signals below 272 K due to a slow isomerization process between two species with lower symmetry, as observed earlier for LnDOTA-like complexes. However, we could not cool the sample without freezing in order to find experimental evidence for the hypothesis. Thus, we could not measure the chemical shift difference for the two sites, and the actual NMR time scale for those nuclei is not known. The doublet signal of the carbonyl carbon atoms changes similarly to the signal of the aliphatic carbon atoms at low temperatures (i.e., sharpening in the range of 272−300 K), but above 300 K, substantial broadening can be observed. The actual NMR time scales of the signals due to the pendant arms are likely defined by the spin−spin coupling constants $^3J_{^1H-^{205}Tl}$. The signal due to the carbonyl groups is in the slow exchange regime at low temperatures and thus it broadens as the temperature increases. The signal due to the $-CH_2-$ carbon nuclei of the pendant arms is, however, in the fast exchange regime at low temperatures, presumably due to a smaller $^3J_{^1H-^{205}Tl}$ coupling.

The $[Tl(dota)]^-$ complex exists in solution as a racemic mixture of the TSAP′ $\Lambda(\lambda\lambda\lambda\lambda)/\Delta(\delta\delta\delta\delta)$ enantiomeric pair, whereas no significant populations of the SAP′ isomers could be detected by NMR spectroscopy. Thus, the exchange process revealed by the ^{13}C NMR data can be attributed to a $\Lambda(\lambda\lambda\lambda\lambda) \leftrightarrow \Delta(\delta\delta\delta\delta)$ interconversion, which represents a simple case of a two-site exchange between equally populated sites. This process involves both the inversion of the macrocyclic unit $[(\lambda\lambda\lambda\lambda) \leftrightarrow (\delta\delta\delta\delta)]$ and the rotation of the four acetate pendant arms $[\Lambda \leftrightarrow \Delta]$, as described previously in detail for Ln^{3+} dota-like complexes.[56] Since the temperature dependence of the signals at 53.6 and 49.2 ppm covers both the fast and slow exchange regimes, we used these resonances to perform a quantitative band-shape analysis of the exchange process, which provides the exchange rates k_{ex} at every temperature. The agreement between the experimental and simulated spectra is excellent (Figure 10).

The temperature dependence of the evaluated time constants was subsequently used to obtain the activation parameters for the exchange process using the Eyring−Polányi equation (Figure S3, Supporting Information). The results are compared to those obtained for related $dota^{4-}$ complexes in Table 3.

The activation enthalpy ($\Delta H^{\ddagger}$) determined for $[Tl(dota)]^-$ falls between the values reported for $[Bi(dota)]^-$ and $[Lu(dota)]^-$. However, the different signs of the activation entropy obtained for the latter two complexes and the small positive $\Delta S^{\ddagger}$ value determined for $[Tl(dota)]^-$ result in relatively similar activation free energies at 298 K ($\Delta G^{\ddagger}_{298}$). The $[Lu(dota)]^-$ complex exists in solution as a mixture of the eight-coordinate TSAP′ isomer and the nine-coordinate SAP form, and activation parameters for both the ring-inversion and arm-rotation processes could be obtained.[2b] Thus, the large positive activation energy obtained for this complex might be related to the expulsion of the coordinated water molecule in the transition state responsible for the $\Lambda(\lambda\lambda\lambda\lambda) \leftrightarrow \Delta(\delta\delta\delta\delta)$ interconversion. For $[Tl(dota)]^-$, $\Delta S^{\ddagger}$ takes a relatively small positive value, which is likely related to the rearrangement of the hydration shell during the interconversion process.

To obtain a more detailed information on the mechanism responsible for the enantiomerization process in $[Tl(dota)]^-$, we performed a computational investigation of the ring-inversion and arm-rotation processes. According to our calculations performed in aqueous solution at the B3LYP/CRENBL/6-31+G(d,p) level, the inversion of the macrocyclic ring is a four-step process involving the stepwise inversion of each of the four five-membered chelate rings formed by the coordination of the macrocyclic moiety. In each of these steps, one of the chelate rings changes its configuration from δ to λ (or vice versa) through a transition state in which the H−C−C−H units adopt a nearly eclipsed conformation. Similar four-step processes have been obtained previously using HF and DFT calculations for different Ln^{3+} complexes with cyclen-based ligands.[57] Due to the symmetry properties of the $[Tl(dota)]^-$ complex (C_4 point group), two different routes are possible for the inversion of the second and third chelate rings (Figure 11), as once the first chelate is inverted the second step may proceed via inversion of a chelate ring either in opposite (TS2a and TS3a) or adjacent (TS2b and TS3b) position at the macrocyclic ring with respect to the former. According to our calculations, the lowest-energy pathway corresponds to that proceeding through TS3b, which provides an activation Gibbs free energy for the ring-inversion process of $\Delta G^{\ddagger}$ = 60.8 kJ mol^{-1} at 298 K.

Contrary to the ring-inversion process, the arm-rotation pathway is a single-step process involving the simultaneous rotation of the four pendant arms of the ligand. The structure of the TS (TS5, Figure 11) is quite distorted, with four different Tl−N distances in the range 2.50−2.75 Å and four Tl−O distances ranging between 2.30 and 2.37 Å. The activation free energy for the arm-rotation process amounts to $\Delta G^{\ddagger}_{298}$ = 67.5 kJ mol^{-1} and thus the arm-rotation process likely represents the rate-determining step for the $\Lambda(\lambda\lambda\lambda\lambda) \leftrightarrow \Delta(\delta\delta\delta\delta)$ inter-

DOI: 10.1021/acs.inorgchem.5b00458
Inorg. Chem. 2015, 54, 5426−5437

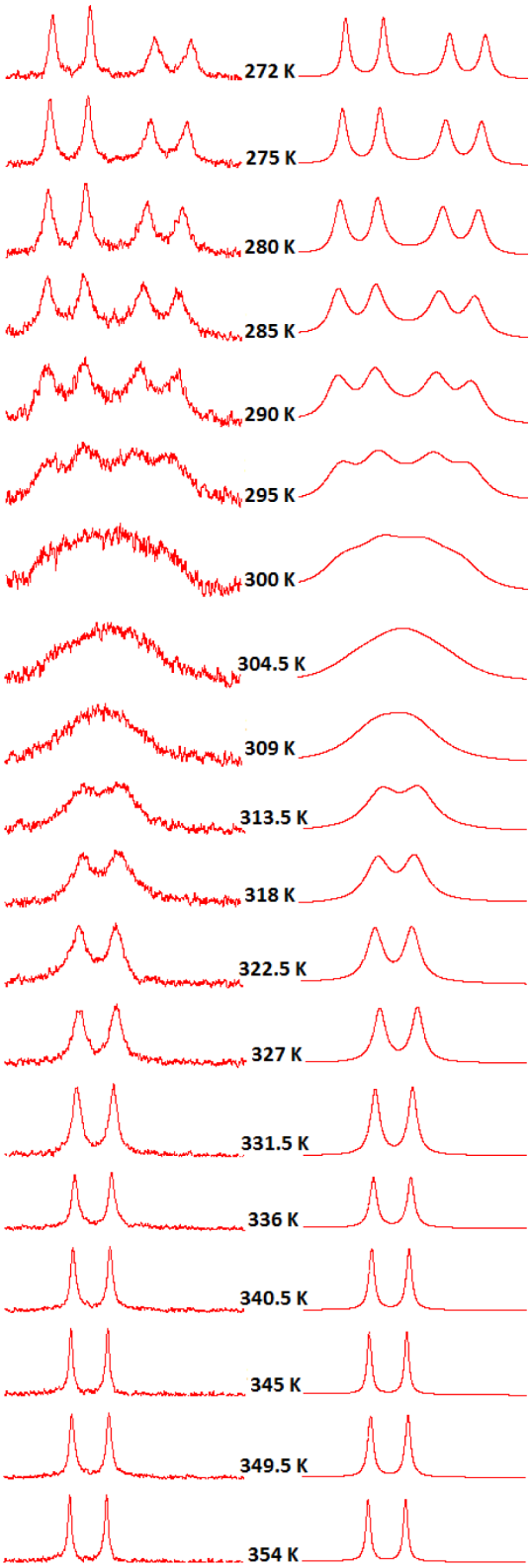

Figure 10. Experimental (left) and simulated (right) ^{13}C NMR spectra of $[Tl(dota)]^-$ at varying temperatures.

conversion in $[Tl(dota)]^-$. The $\Delta H^{\ddagger}$ and $\Delta S^{\ddagger}$ values calculated for the arm-rotation pathway (Table 3) show a very good agreement with the experimental values, which provides additional support for this hypothesis. In contrast, the ring-inversion path provides negligible activation entropy.

Table 3. Activation Parameters Obtained for the $\Lambda(\lambda\lambda\lambda\lambda) \leftrightarrow \Delta(\delta\delta\delta\delta)$ Interconversion in $[Tl(dota)]^-$ and Related Systems

		$\Delta H^{\ddagger}$/ kJ mol^{-1}	$\Delta S^{\ddagger}$/ J K^{-1} mol^{-1}	$\Delta G^{\ddagger}_{298}$/ kJ mol^{-1}
$[Tl(dota)]^-$	exp	66 ± 2	+23 ± 6	59 ± 2
	calcd[a]	73.2	+19.2	67.5
$[Bi(dota)]^-$[b]	exp	40	−76 ± 15	63
$[Lu(dota)]^-$[c]	exp	101	+116	66

[a]Values are obtained for the arm-rotation process with DFT calculations in aqueous solution at the B3LYP/CRENBL/6-31+G(d,p) level. [b]From ref 5. [c]From ref 2b.

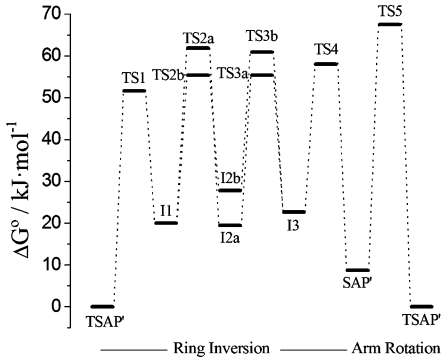

Figure 11. Relative free energies of minima, intermediates (labeled I) and transition states (labeled TS) involved in the $\Lambda(\lambda\lambda\lambda\lambda) \leftrightarrow \Delta(\delta\delta\delta\delta)$ interconversion process of $[Tl(dota)]^-$ calculated in aqueous solution at the B3LYP/CRENBL/6-31+G(d,p) level.

CONCLUSIONS

The X-ray and spectroscopic study presented in this work points to a very compact structure of the $[Tl(dota)]^-$ complex, which presents TSAP′ coordination around the metal ion. This complex does not react with Br^- or OH^- anions, as observed for the $[Tl(edta)]^-$ analogue, and forms a weak mixed complex with cyanide. The $[Tl(dota)]^-$ complex is very inert, the dissociation is a proton-assisted process, and the half-life of dissociation is on the order of 10^9 h at neutral pH. The ^1H, ^{13}C, and ^{205}Tl NMR spectra provided $^3J_{H-^{205}Tl}$ spin−spin coupling constants of up to ∼575 Hz and $^2J_{^{13}C-^{205}Tl}$ values of ca. 60−160 Hz. The large values of these coupling constants reflect an important degree of covalency of the Tl−ligand bonds, which is probably responsible, at least in part, for the robustness of the complex. A detailed study of the dynamic behavior of $[Tl(dota)]^-$ in solution indicates that the rotation of the pendant arms of the ligand most likely represents the rate-determining step of the $\Lambda(\lambda\lambda\lambda\lambda) \leftrightarrow \Delta(\delta\delta\delta\delta)$ interconversion.

ASSOCIATED CONTENT

Supporting Information

Figure S1: Scheme of the $Tl(ClO_4)_3$ electrolysis device. Figure S2: 400 MHz $^1H-^{13}C$ HSQC spectrum. Figure S3: Modified Eyring diagram. Figure S4: ^1H NMR spectra of 0.1 M $[Tl(dota)]^-$ at varying temperatures. Figure S5: 288.5 MHz ^{205}Tl NMR spectrum of $[Tl(dota)]^-$ at 268 K. Figure S6: Packing diagram of $\{C(NH_2)_3\}[Tl(dota)]\cdot H_2O$, view normal to (100). Table S1: Cartesian coordinates of the intermediates and transition states of the $[Tl(dota)]^-$ system optimized at the B3LYP/CRENBL/6-31+G(d,p) level using the polarizable continuum model (water solvent). Crystal structure analysis.

DOI: 10.1021/acs.inorgchem.5b00458
Inorg. Chem. 2015, 54, 5426−5437

The Supporting Information is available free of charge on the ACS Publications website at DOI: 10.1021/acs.inorgchem.5b00458.

AUTHOR INFORMATION

Corresponding Author

*E-mail: imre.toth@science.unideb.hu.

Notes

The authors declare no competing financial interest.

ACKNOWLEDGMENTS

The research was supported by the EU and cofinanced by the European Social Fund under the project ENVIKUT (TÁMOP-4.2.2.A-11/1/KONV-2012-0043). The authors also acknowledge the support of the Hungarian Scientific Research Fund (OTKA K-109029 and K-84291). This work was partially supported by the European Union and the European Social Fund through project Supercomputer, the national virtual lab (grant no. TÁMOP-4.2.2.C-11/1/KONV- 2012-0010) (M.P.). This research was performed within the framework of the EU COST Action TD1004 "Theragnostics Imaging and Therapy: An Action to Develop Novel Nanosized Systems for Imaging-Guided Drug Delivery". C.P.-I. thanks Centro de Supercomputación de Galicia (CESGA) for providing the computer facilities.

REFERENCES

(1) (a) Stasiuk, G. J.; Long, N. J. *Chem. Commun.* **2013**, *49*, 2732−2746. (b) Liu, S. *Adv. Drug Delivery Rev.* **2008**, *60*, 1347−1370. (c) Lattuada, L.; Barge, A.; Cravotto, G.; Giovenzana, G. B.; Tei, L. *Chem. Soc. Rev.* **2011**, *40*, 3019−3049. (d) Viswanathan, S.; Kovacs, Z.; Green, K. N.; Ratnakar, S. J.; Sherry, A. D. *Chem. Rev.* **2010**, *110*, 2960−3018. (e) Tanaka, K.; Fukase, K. *Org. Biomol. Chem.* **2008**, *6*, 815−828.

(2) (a) Benetollo, F.; Bombieri, G.; Calabi, L.; Aime, S.; Botta, M. *Inorg. Chem.* **2003**, *42*, 148−157. (b) Aime, S.; Barge, A.; Botta, M.; Fasano, M.; Ayala, J. D.; Bombieri, G. *Inorg. Chim. Acta* **1996**, *246*, 423−429.

(3) Parker, D.; Pulukkody, K.; Smith, F. C.; Batsanov, A.; Howard, J. A. K. *J. Chem. Soc., Dalton Trans.* **1994**, 689−693.

(4) Heppeler, A.; André, J. P.; Buschmann, I.; Wang, X.; Reubi, J.-C.; Henning, M.; Kaden, T. A.; Maecke, H. R. *Chem.—Eur. J.* **2008**, *14*, 3026−3034.

(5) Csajbok, E.; Baranyai, Z.; Banyai, I.; E. Brücher, E.; Kiraly, R.; Müller-Fahrnow, A.; Platzek, J.; Radüchel, B.; Schäfer, M. *Inorg. Chem.* **2003**, *42*, 2342−2349.

(6) Anderson, O. P.; Reibenspies, J. H. *Acta Crystallogr.* **1996**, *C52*, 792−795.

(7) Burai, L.; Tóth, E.; Moreau, G.; Sour, A.; Scopelliti, R.; Merbach, A. E. *Chem.—Eur. J.* **2003**, *9*, 1394−1404.

(8) Riesen, A.; Zehnder, M.; Kaden, T. A. *Acta Crystallogr.* **1991**, *C47*, 531−533.

(9) Chang, C. A.; Francesconi, L. C.; Malley, M. F.; Kumar, K.; Gougoutas, J. Z.; Tweedle, M. F. *Inorg. Chem.* **1993**, *32*, 3501−3508.

(10) Riesen, A.; Zehnder, M.; Kaden, T. A. *Helv. Chim. Acta* **1986**, *69*, 2067−2073.

(11) Viola-Villegas, N.; Doyle, R. P. *Coord. Chem. Rev.* **2009**, *253*, 1906−1925.

(12) (a) Kubicek, V.; Havlickova, J.; Kotek, J.; Tircso, G.; Hermann, P.; Toth, E.; Lukes, I. *Inorg. Chem.* **2010**, *49*, 10960−10969. (b) Drahos, B.; Kubicek, V.; Bonnet, C. S.; Hermann, P.; Lukes, I.; Toth, E. *Dalton Trans.* **2011**, *40*, 1945−1951. (c) Toth, E.; Brucher, E.; Lazar, I.; Toth, I. *Inorg. Chem.* **1994**, *33*, 4070−4076. (d) Brucher, E.; Laurenczy, G.; Makra, Z. *Inorg. Chim. Acta* **1987**, *139*, 141−142.

(13) (a) Voracova, I.; Vanek, J.; Pasulka, J.; Strelcova, Z.; Lubal, P.; Hermann, P. *Polyhedron* **2013**, *61*, 99−104. (b) Pniok, M.; Kubicek, V.; Havlickova, J.; Kotek, J.; Sabatie-Gogova, A.; Plutnar, J.; Huclier-Markai, S.; Hermann, P. *Chem.—Eur. J.* **2014**, *20*, 7944−7955.

(14) (a) Wang, X.; Jin, T.; Comblin, V.; Lopez-Mut, A.; Merciny, E.; Desreux, J. F. *Inorg. Chem.* **1992**, *31*, 1095−1099. (b) Wu, S. L.; Horrocks, W., Jr. *Inorg. Chem.* **1995**, *34*, 3724−3732. (c) Moreau, J.; Guillon, E.; Pierrard, J.-C.; Rimbault, J.; Port, M.; Aplincourt, M. *Chem.—Eur. J.* **2004**, *10*, 5218−5232.

(15) Martins, A. F.; Prata, M. I. M.; Rodrigues, S. P. J.; Geraldes, C.; Riss, P. J.; Amor-Coarasa, A.; Burchardt, C.; Kroll, C.; Rösch, F. *Contrast Media Mol. Imaging* **2013**, *8*, 265−273.

(16) (a) Benazeth, S.; Purans, J.; Chalbot, M.-C.; Nguyen-van-Duong, M. K.; Nicolas, L.; Keller, F.; Gaudemer, A. *Inorg. Chem.* **1998**, *37*, 3667−3674. (b) Aime, S.; Botta, M.; Ermondi, G. *Inorg. Chem.* **1992**, *31*, 4291−4299. (c) Hoeft, S.; Roth, K. *Chem. Ber.* **1993**, *126*, 869−873. (d) Fusaro, L.; Luhmer, M. *Inorg. Chem.* **2014**, *53*, 8717−8722. (e) Aime, S.; Botta, M.; Fasano, M.; Marques, M. P. M.; Geraldes, C. F. G. C.; Purbanz, D.; Merbach, A. E. *Inorg. Chem.* **1997**, *36*, 2059−2068. (f) Mayer, F.; Platas-Iglesias, C.; Helm, L.; Peters, J. A.; Djanashvili, K. *Inorg. Chem.* **2012**, *51*, 170−178. (g) Esteban-Gomez, D.; de Blas, A.; Rodriguez-Blas, T.; Helm, L.; Platas-Iglesias, C. *ChemPhysChem* **2012**, *13*, 3640−3650. (h) Powell, D. H.; Ni Dhubhghaill, O. M.; Pubanz, D.; Helm, L.; Lebedev, Y. S.; Schlaepfer, W.; Merbach, A. E. *J. Am. Chem. Soc.* **1996**, *118*, 9333−9346.

(17) Musso, S. Doctoral and Habilitation Theses, ETH Zürich, Switzerland, 1993; http://dx.doi.org/10.3929/ethz-a-000695797.

(18) Tóth, I.; Győri, B. Thallium: Inorganic Chemistry; In *Encyclopedia of Inorganic Chemistry*, 2nd ed.; King, R. B., Ed.; Wiley: Hoboken, NJ, 2005; Vol. *8*, pp 4824−4835.

(19) Anderegg, G. *Critical Survey of Stability Constants of EDTA Complexes*, IUPAC Chemical Data Series 14; Pergamon Press: Oxford, England, 1977.

(20) Toth, I.; Brucher, E.; Zekany, L.; Veksin, V. *Polyhedron* **1989**, *8*, 2057−2064.

(21) Bottari, E.; Anderegg, G. *Helv. Chim. Acta* **1967**, *50*, 2341−2349.

(22) Dozsa, L.; Szabo, A.; Beck, M. T. *Acta Chim. Acad. Sci. Hung.* **1971**, *67*, 189−194.

(23) (a) Reilley, C. N.; Scribner, W. G.; Temple, C. *Anal. Chem.* **1956**, *28*, 450−454. (b) Tanaka, N.; Ogino, H. *Bull. Chem. Soc. Jpn.* **1965**, *38*, 1054.

(24) Blixt, J.; Glaser, J.; Solymosi, P.; Toth, I. *Inorg. Chem.* **1992**, *31*, 5288−5297.

(25) Tóth, I.; Reiter, I.; Brücher, E.; Vince, L. In Abstracts of XIX International Conference on Solution Chemistry, Lund, August 15−18, 1988; p 109, ISBN 91-7970-299-6.

(26) Hijnen, N. M.; de Vries, A.; Blange, R.; Burdinski, D.; Grüll, H. *Nucl. Med. Biol.* **2011**, *38*, 585−592.

(27) Horvat, H. *Investigation of the decomposition of the [NaTl(edta)]-complex*. Thesis, University of Debrecen, Debrecen, Hungary, 2010; https://dea.lib.unideb.hu/dea/handle/2437/101064.

(28) Glaser, J. Ph.D. Thesis, The Royal Institute of Technology (KTH), Stockholm, 1981; p 15.

(29) Irving, H. M.; Miles, M. G.; Pettit, L. D. *Anal. Chim. Acta* **1967**, *38*, 475−488.

(30) Reeves, L. W.; Shaw, K. N. *Can. J. Chem.* **1970**, *48*, 3641−3643.

(31) Kathó, Á.; Bényei, A. C.; Joó, F.; Sági, M. *Adv. Synth. Catal.* **2002**, *344*, 278−282.

(32) Altomare, A.; Cascarano, G.; Giacovazzo, C.; Guagliardi, A. *J. Appl. Crystallogr.* **1993**, *26*, 343−350.

(33) Sheldrick, G. M. *Acta Crystallogr.* **2008**, *A64*, 112−122.

(34) (a) Becke, A. D. *J. Chem. Phys.* **1993**, *98*, 5648−5652. (b) Lee, C.; Yang, W.; Parr, R. G. *Phys. Rev. B* **1988**, *37*, 785−789.

(35) Frisch, M. J.; Trucks, G. W.; Schlegel, H. B.; Scuseria, G. E.; Robb, M. A.; Cheeseman, J. R.; Scalmani, G.; Barone, V.; Mennucci, B.; Petersson, G. A.; Nakatsuji, H.; Caricato, M.; Li, X.; Hratchian, H. P.; Izmaylov, A. F.; Bloino, J.; Zheng, G.; Sonnenberg, J. L.; Hada, M.; Ehara, M.; Toyota, K.; Fukuda, R.; Hasegawa, J.; Ishida, M.; Nakajima, T.; Honda, Y.; Kitao, O.; Nakai, H.; Vreven, T.; Montgomery, J. A., Jr.; Peralta, J. E.; Ogliaro, F.; Bearpark, M.; Heyd, J. J.; Brothers, E.; Kudin, K. N.; Staroverov, V. N.; Kobayashi, R.; Normand, J.; Raghavachari, K.;

DOI: 10.1021/acs.inorgchem.5b00458
Inorg. Chem. 2015, 54, 5426−5437

Rendell, A.; Burant, J. C.; Iyengar, S. S.; Tomasi, J.; Cossi, M.; Rega, N.; Millam, J. M.; Klene, M.; Knox, J. E.; Cross, J. B.; Bakken, V.; Adamo, C.; Jaramillo, J.; Gomperts, R.; Stratmann, R. E.; Yazyev, O.; Austin, A. J.; Cammi, R.; Pomelli, C.; Ochterski, J. W.; Martin, R. L.; Morokuma, K.; Zakrzewski, V. G.; Voth, G. A.; Salvador, P.; Dannenberg, J. J.; Dapprich, S.; Daniels, A. D.; Farkas, O.; Foresman, J. B.; Ortiz, J. V.; Cioslowski, J.; Fox, D. J. *Gaussian 09*, revision A.01; Gaussian, Inc.: Wallingford, CT, 2009.
(36) Ross, R. B.; Powers, J. M.; Atashroo, T.; Ermler, W. C.; LaJohn, L. A.; Christiansen, P. A. *J. Chem. Phys.* **1990**, *93*, 6654−6670.
(37) (a) Peng, C.; Ayala, P. Y.; Schlegel, H. B.; Frisch, M. J. *J. Comput. Chem.* **1996**, *17*, 49−56. (b) Peng, C.; Schlegel, H. B. *Isr. J. Chem.* **1994**, *33*, 449−454.
(38) Wolinski, K.; Hilton, J. F.; Pulay, P. *J. Am. Chem. Soc.* **1990**, *112*, 8251−8260.
(39) Tomasi, J.; Mennucci, B.; Cammi, R. *Chem. Rev.* **2005**, *105*, 2999−3093.
(40) Parker, D.; Dickins, R. S.; Puschmann, H.; Crossland, C.; Howard, J. A. K. *Chem. Rev.* **2002**, *102*, 1977−2010.
(41) Shannon, R. D. *Acta Crystallogr.* **1976**, *A32*, 751−767.
(42) Aime, S.; Barge, A.; Benetollo, F.; Bombieri, G.; Botta, M.; Uggeri, F. *Inorg. Chem.* **1997**, *36*, 4287−4289.
(43) (a) Vojtisek, P.; Cigler, P.; Kotek, J.; Rudovsky, J.; Hermann, P.; Lukes, I. *Inorg. Chem.* **2005**, *44*, 5591−5599. (b) Kotek, J.; Rudovsky, J.; Hermann, P.; Lukes, I. *Inorg. Chem.* **2006**, *45*, 3097−3102.
(44) Parr, R. G.; Pearson, R. G. *J. Am. Chem. Soc.* **1983**, *105*, 7512−7516.
(45) Glaser, J. In *Advances in Inorganic Chemistry*; Sykes, G., Ed.; Academic Press: San Diego, CA, 1995; Vol. *43*, pp 1−78.
(46) Jalilehvand, F.; Maliarik, M.; Sandström, M.; Mink, J.; Persson, I.; Persson, P.; Tóth, I.; Glaser, J. *Inorg. Chem.* **2001**, *40*, 3889−3899.
(47) Blixt, J.; Dubey, R. K.; Glaser, J. *Inorg. Chem.* **1991**, *30*, 2824−2826.
(48) Nagy, P.; Joszai, R.; Fabian, I.; Toth, I.; Glaser, J. *J. Mol. Liq.* **2005**, *118*, 195−207.
(49) Banyai, I.; Glaser, J. *J. Am. Chem. Soc.* **1990**, *112*, 4703−4710.
(50) Banyai, I.; Blixt, J.; Glaser, J.; Toth, I. *Acta Chem. Scand.* **1992**, *46*, 138−141.
(51) (a) Karplus, M. *J. Am. Chem. Soc.* **1963**, *85*, 2870−2871. (b) Geraldes, C. F. G. C.; Sherry, A. D.; Kiefer, G. E. *J. Magn. Reson.* **1992**, *97*, 290−304.
(52) Rodríguez-Rodríguez, A.; Esteban-Gomez, D.; de Blas, A.; Rodriguez-Blas, T.; Fekete, M.; Botta, M.; Tripier, R.; Platas-Iglesias, C. *Inorg. Chem.* **2012**, *51*, 2509−2521.
(53) Rodríguez-Rodríguez, A.; Esteban-Gomez, D.; de Blas, A.; Rodriguez-Blas, T.; Botta, M.; Tripier, R.; Platas-Iglesias, C. *Inorg. Chem.* **2012**, *51*, 13419−13429.
(54) van Wüllen, C. *J. Chem. Phys.* **2012**, *136*, 114110.
(55) Purgel, M.; Baranyai, Z.; de Blas, A.; Rodriguez-Blas, T.; Banyai, I.; Platas-Iglesias, C.; Toth, I. *Inorg. Chem.* **2010**, *49*, 4370−4382.
(56) Platas-Iglesias, C. *Eur. J. Inorg. Chem.* **2012**, 2023−2033.
(57) (a) Regueiro-Figueroa, M.; Estabn-Gómez, D.; de Blas, A.; Rodríguez-Blas, T.; Platas-Iglesias, C. *Eur. J. Inorg. Chem.* **2010**, 3586−3595. (b) Regueiro-Figueroa, M.; Bensenane, B.; Ruscsák, E.; Esteban-Gómez, D.; Charbonnière, L. J.; Tircsó, G.; Tóth, I.; de Blas, A.; Rodríguez-Blas, T.; Platas-Iglesias, C. *Inorg. Chem.* **2011**, *50*, 4125−4141. (c) Lima, L. M. P.; Lecointre, A.; Morfin, J.-F.; de Blas, A.; Visvikis, D.; Charbonnière, L. J.; Platas-Iglesias, C.; Tripier, R. *Inorg. Chem.* **2011**, *50*, 12508−12521. (d) Cosentino, U.; Villa, A.; Pitea, D.; Moro, G.; Barone, V.; Maiocchi, A. *J. Am. Chem. Soc.* **2002**, *124*, 4901−4909. (e) Natrajan, L. S.; Khoabane, N. M.; Dadds, B. L.; Muryn, C. A.; Pritchard, R. G.; Heath, S. L.; Kenwright, A. M.; Kuprov, I.; Faulkner, S. *Inorg. Chem.* **2010**, *49*, 7700−7709. (f) Di Vaira, M.; Stoppioni, P. *New J. Chem.* **2002**, *26*, 136−144.

DOI: 10.1021/acs.inorgchem.5b00458
Inorg. Chem. 2015, 54, 5426−5437